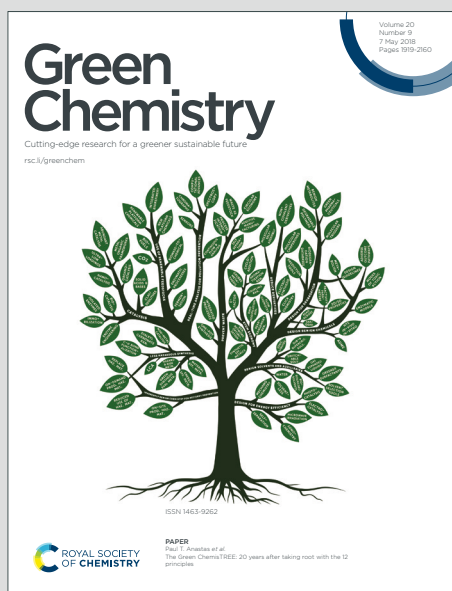


# Green Chemistry

Cutting-edge research for a greener sustainable future

Accepted Manuscript

This article can be cited before page numbers have been issued, to do this please use: X. Hu, Y. Liu, H. Huang, B. Huang, G. Chai and Z. Xie, *Green Chem.*, 2020, DOI: 10.1039/C9GC03781K.



This is an Accepted Manuscript, which has been through the Royal Society of Chemistry peer review process and has been accepted for publication.

Accepted Manuscripts are published online shortly after acceptance, before technical editing, formatting and proof reading. Using this free service, authors can make their results available to the community, in citable form, before we publish the edited article. We will replace this Accepted Manuscript with the edited and formatted Advance Article as soon as it is available.

You can find more information about Accepted Manuscripts in the [Information for Authors](#).

Please note that technical editing may introduce minor changes to the text and/or graphics, which may alter content. The journal's standard [Terms & Conditions](#) and the [Ethical guidelines](#) still apply. In no event shall the Royal Society of Chemistry be held responsible for any errors or omissions in this Accepted Manuscript or any consequences arising from the use of any information it contains.

# Template-free Synthesis of Graphene-like Carbons as Efficient Carbocatalysts for Selective Oxidation of Alkanes

*Xiang Hu<sup>1</sup>, Yuchuan Liu<sup>1</sup>, Haitao Huang<sup>1</sup>, Baobing Huang<sup>1</sup>, Guoliang Chai<sup>2\*</sup> and Zailai Xie<sup>1\*</sup>*

1. College of Chemistry, Fuzhou University, 2 Xueyuan Road, Fuzhou 350116, China

Corresponding author. Email: zlxie@fzu.edu.cn, Tel: +(86)-591-22866102

2. State Key Laboratory of Structural Chemistry, Fujian Institute of Research on the Structure of Matter, Chinese Academy of Sciences (CAS), Fuzhou, 350002, China

Corresponding author. Email: g.chai@fjirsm.ac.cn

## Abstract

Selective oxidation of aromatic alkanes by C-H activation is one of the key reactions in organic synthesis and chemical industry. It is of particular interest to activate C-H bond to get high-value added products under mild conditions by using sustainable carbocatalysts. Herein, we report a sustainable, green and template-free strategy towards the fabrication of N-doped and N/S codoped carbon nanosheets by metal-free carbonization of bioprecursor guanine and guanine sulfate. The occurrence of thin and N/S codoped carbon nanosheets was induced by multiple interactions of nucleobase. Benefiting from the unique textural structure of the as-synthesized carbons, including ultrathin thickness, optimal porosity, rich structural defects and synergistic coupling effect of multiple dopants, the carbon nanosheet delivers a high catalytic performance with 85% ethylbenzene conversion and 98% selectivity of acetophenone at 80 °C after 4 h reaction, which outperforms other equivalent benchmarks (e.g. 8.5 times in conversion

and 3.2 times in selectivity higher than oxidized carbon nanotubes). Density functional theory simulations indicate that the oxidation of ethylbenzene is catalyzed by synergic effect of p-N/S and g-N/S catalysts *via* OH radical mechanism. This N/S codoped strategy provides guidance for the design of carbon-based catalysts for selective oxidation of other alkanes.

**Keywords:** selective oxidation; N/S codoped carbon nanosheets; ethylbenzene; OH radical

## Introduction

Selective oxidation of aromatic alkanes via C-H bond activation is one key important reactions in organic synthesis and chemical industry, since it enables the production of high value-added platform molecules such as cyclohexanone, cyclohexanol, and organic acids.<sup>1-5</sup> General approaches for efficient C-H bond activation are usually mediated by employing of transition metals or organometallic compounds as heterogeneous or homogeneous catalysts.<sup>6, 7</sup> As of now, the transition metal or organometallic centers, such as Ru<sup>8</sup>, Pt<sup>9</sup>, Au<sup>10</sup>, Pd<sup>11</sup>, Co<sup>12, 13</sup> etc. have demonstrated grand potential in C-H activation. In spite of highly efficiency of metal-based catalysts, the high cost and limited resource have prompted worldwide efforts to explore non-noble metal or metal-free catalysts and more environment-friendly process.<sup>14</sup> In view of these, it is desirable to develop recyclable heterogeneous metal-free catalysts with high activity and low cost.

The past decade have witnessed the rapid development of the carbon-mediated reactions which was also called carbocatalysis and has gained enormous attention due to the economical and sustainable nature of the catalyst.<sup>15-18</sup> So far, a couple of reactions such as oxidative dehydrogenation, oxidative coupling, catalytic oxidation, reduction, and transesterification reactions,<sup>1, 19-26</sup> can be effectively catalyzed by carbon materials. As the pioneering work of carbocatalysis, Su *et al.* discovered that nanocarbons are an efficient metal-free catalyst to activate short chain alkanes, in which carbonyl group was confirmed to be the active origin.<sup>27</sup> Ma *et al.* reported that graphitic-type sites in layered carbon catalysts is pivotal for the C-H bond activation reaction, while nitrogen dopant did not participant in the activation of reactant.<sup>28</sup> After that, considerable efforts have focused on improving the oxidation performance based on carbocatalysts by identifying and exposing active sites, as well as surface engineering.<sup>18, 19, 29</sup> Apart from oxygen functional groups, structural defects and doped heteroatoms are also potential active centers or have significant effect on catalytic activity.<sup>18, 27, 30-32</sup>

Indeed, heteroatoms-doped nanocarbons have been widely investigated as carbocatalysts to improve catalytic performance of C-H bond activation.<sup>29, 33, 34</sup> Nitrogen, phosphorus and sulfur were generally used as electron donors to modulate the  $\pi$ -conjugated system at the periphery of carbon structures.<sup>35</sup> The altered spin distribution or charge of the sp<sup>2</sup> carbon by heteroatom doping facilitates molecules adsorption by electrostatic interaction or hydrogen bonding like S-O $\cdots$ H, and subsequently the C-H bond breaking.<sup>36</sup> Meanwhile, the intrinsic defects (e.g., vacancies, Stone-Wales defects or edges) can also break the electron-hole symmetry, and inducing the radical production from oxidant decomposition.<sup>37</sup> All above these enable wide spectrum change of the carbons not only in the composition and structure, but also in diversification of catalytic functions and applications. However, despite considerable achievements have been made in recent years, the mechanism interpretation about how multiple heteroatoms affect catalytic properties of carbons is still unclear and the selective oxidation of C-H bonds with high efficiency under mild conditions driven by carbonalysts remains to be explored.

Another key point to boost catalytic activity is to maximum expose active sites. The two dimensional (2D) carbons possess unique advantages which can satisfy this requirement, such as their potentially large surface area (theoretically up to ca. 2600 m<sup>2</sup>/g), capable of providing a 2D area carrying abundant active sites for redox reactions, and easily accessible inner-outer interfaces of the 2D architecture.<sup>38</sup> Such 2D carbons in some cases can serve as a substitute or beneficial complementation of the traditional metals or metal oxides, especially noble metals.<sup>39-42</sup> Although 2D carbon materials are widely investigated, a sustainable, green and template-free strategy to synthesis of well-defined 2D carbon nanosheet has rarely been realized. In this aspect, natural biomolecules could be used as 2D carbon source, as they often appear in the form of supramolecular self-assemblies due to their abundant resources and multiple reaction sites.<sup>43</sup> These natural molecules would self-assemble into various supramolecular

assemblies primarily promoted by non-covalent interactions, such as hydrogen bonding,  $\pi$ - $\pi$  stacking, van der Waals forces.<sup>44</sup> Indeed, we previously reported that their unique molecular morphologies would be transferred into carbon architecture during the carbonization process, and hence providing a facile method to fabricate nanosheets nanostructures.<sup>45, 46</sup>

Herein, we report an occurrence of thin and N/S codoped carbon nanosheets induced by multiple interactions of nucleobase. The as-synthesized carbon nanosheets possess a series of merits, such as relatively high surface area, ultrathin thickness, optimal porosity, rich structural defects and synergistic coupling effect of multiple dopants, which render it suitable for efficient carbocatalysis. To investigate the effect of N/S doping on catalytic activity, control experiments by different pyrolysis temperatures were conducted to screen the optimized catalyst. The selective oxidation of ethylbenzene (EB) with tert-butyl hydroperoxide (TBHP) as oxidant was selected to evaluate the catalytic properties of nanocarbon catalysts for the activated oxidation of C-H bonds. Among all the catalysts, N/S codoped sample that was obtained by thermal pyrolysis at 1000 °C (GS1000) delivers a high catalytic performance with 85% EB conversion and 98% selectivity of acetophenone (AcPO), which is 8.5 times in conversion and 3.2 times in selectivity higher than OCNT under identical condition, better than most of previously reported carbon-based benchmark catalysts. The density functional theory (DFT) simulations indicate that the oxidation of ethylbenzene is catalysed by synergic effect of p-N/S and g-N/S catalysts *via* OH radical mechanism. Moreover, a wide scope of substituted aromatic hydrocarbons could also be smoothly oxidized under mild condition, and the selectivity of corresponding products reached as high as 97%. Given the diversity in the structure of the nucleobase moiety, they represent ideal building blocks for the catalyst-free and metal-free formation of 2D carbon carbocatalysts with enhanced catalytic properties for carbocatalysis.

## Experimental

### *Catalysts synthesis*

For the preparation of the N/S codoped 2D carbons, 30 g guanine and 5.4 mL concentrated sulfuric acid were dispersed into 300 mL deionized water under stirring for 24 h. The prepared precursors were dried and transferred into a tube furnace and pyrolyzed at given temperature for 1 h at a heating rate of 5 °C/min in N<sub>2</sub> flow. Then, the black solids were taken out and calcined for another hour at the same temperature. The powder obtained finally were named as GSX, where X represent the stipulated pyrolysis temperature. Similarly, the N-doped 2D carbons were prepared by direct pyrolysis of guanine at a stipulated temperature for 1 h in N<sub>2</sub> flow at twice, which names as GX (X represent the pyrolysis temperature)

### *Physical characterization*

Nitrogen physisorption measurements were carried out at 77 K by Micromeritics ASAP 2020 plus and ASAP 2060. Powder X-ray diffraction (XRD) patterns were collected by RIGAKU Ultima IV, and diffraction patterns were attained by using Cu K<sub>α</sub> ( $\lambda = 1.5406 \text{ \AA}$ ) radiation at a scanning of 10° min<sup>-1</sup> from 5° to 80°. The Raman spectra were measured by Renishaw inVia with a 532 nm laser excitation. XPS measurement was conducted using ESCALAB 250 with a source gun of Al K<sub>α</sub> with spot size of 500 μm. Scanning electron micrograph (SEM) was acquired by Hitachi S-4800 operated at 15kV. Transmission electron microscopy (TEM) images, high resolution TEM (HRTEM) images, and high angle annular dark field scanning TEM (HAADF-STEM) images were recorded on a FEI Talos F200S G2 microscope operated at 200 kV.

### *Catalytic experiments*

All reactions were carried out in a 5 mL round-bottom flask. Typically, 10 mg catalysts, 1 mL 70% TBHP, 2 mL H<sub>2</sub>O and 1 mmol ethylbenzene were added to flask and the reaction was proceeded in an 80 °C oil bath for 4 h. Anisole was added to the solution as internal standard after the reaction. Gas chromatography and GC-MS were

used to analyze the reaction mixture.

### *Simulation methods*

The density functional theory (DFT) simulations were performed by PWSCF code in Quantum ESPRESSO to investigate the reaction mechanisms.<sup>47</sup> The generalized gradient approximation of Perdew-Burke-Ernzerhof (GGA-PBE) was adopted for exchange correlation functional in DFT simulations.<sup>48</sup> The kinetic energy cutoffs for the wavefunction and the charge were set to 40 Ry and 400 Ry, respectively. Spin polarization was taken into account for all the simulations. The lattice parameters parallel to the graphene nanosheet are about  $12.35 \text{ \AA} \times 20 \text{ \AA}$ , and the vacuum region perpendicular to the graphene nanosheet is larger than  $10.00 \text{ \AA}$ . The k-point sampling in the Brillouin zone is set to  $3 \times 1 \times 1$ . Semiempirical Grimme's DFT-D2 method was adopted to describe Van der Waals correction.<sup>49</sup>

## Results and discussion

### Catalyst synthesis and characterization

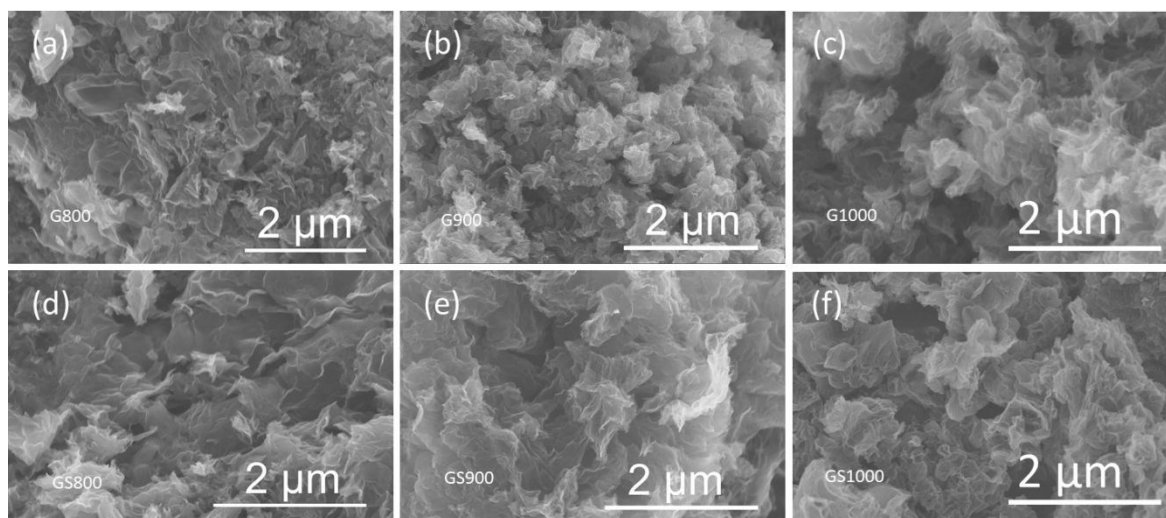


**Figure 1.** The SEM images of different catalysts: (a): G800; (b): G900; (c): G1000; (d): GS800; (e): GS900; (f): GS1000.

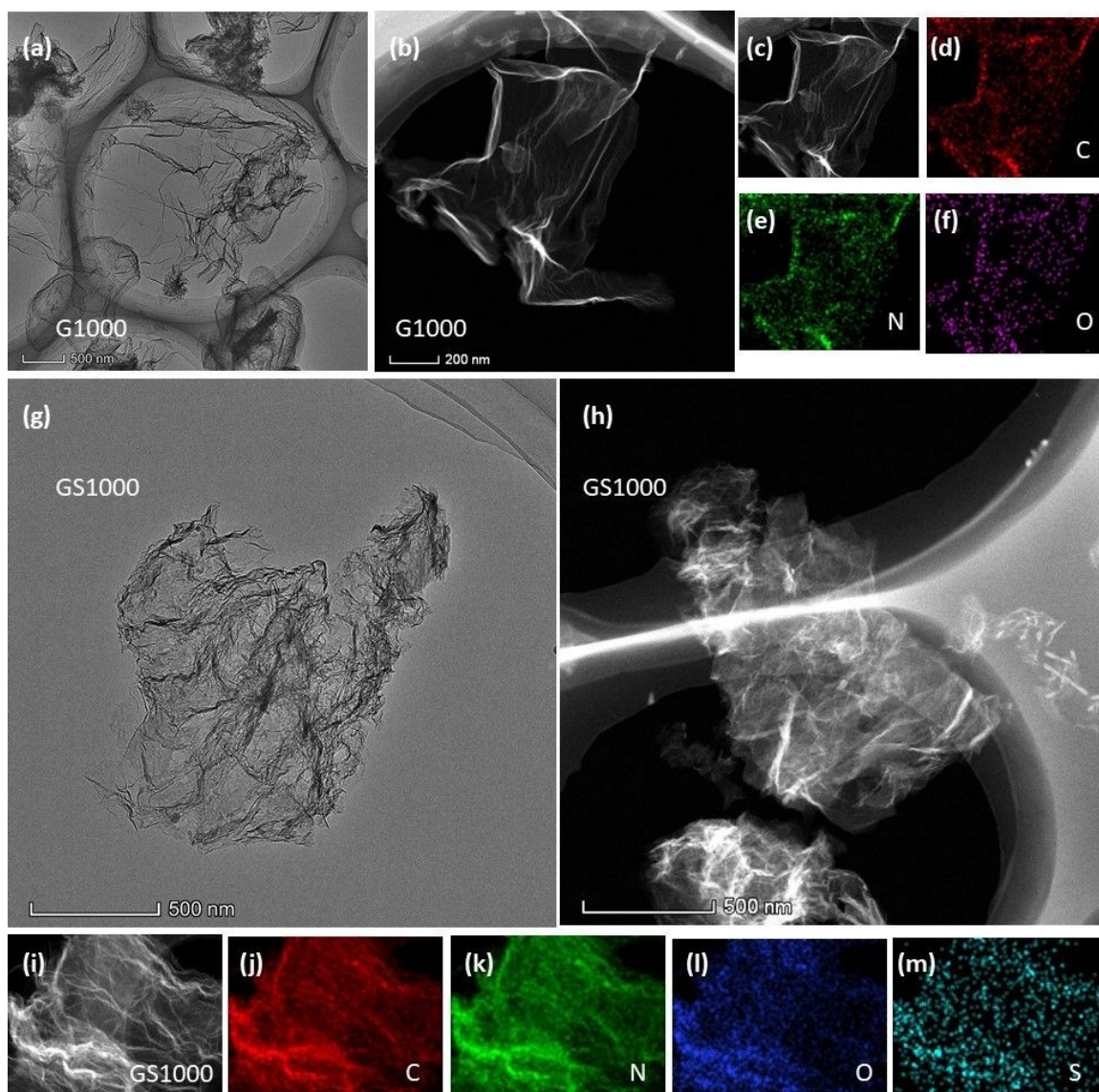


**Figure 2.** The TEM images of G1000 and GS1000, and the corresponding EDS element mapping of C, N, O and S.

Scanning electron microscopy (SEM) images show that all of the carbons have typical sheet-like morphologies with uniformity and thin properties, no matter which temperature (800-1000 °C) used and with or without S doping (Figure 1). Transmission electron microscopy (TEM) images further manifest the formation of graphene-like structures, which are very transparent and curly (Figure 2). Moreover, the elemental mapping images reveal that C, N, and O elements are uniformly distributed over the

skeletons of both G1000 and GS1000, meanwhile S element has been doped evenly into the GS1000 skeleton. It is supposed that such heteroatom-doped properties combined with the unique 2D architecture will be very suitable for heterogeneous catalytic reactions.

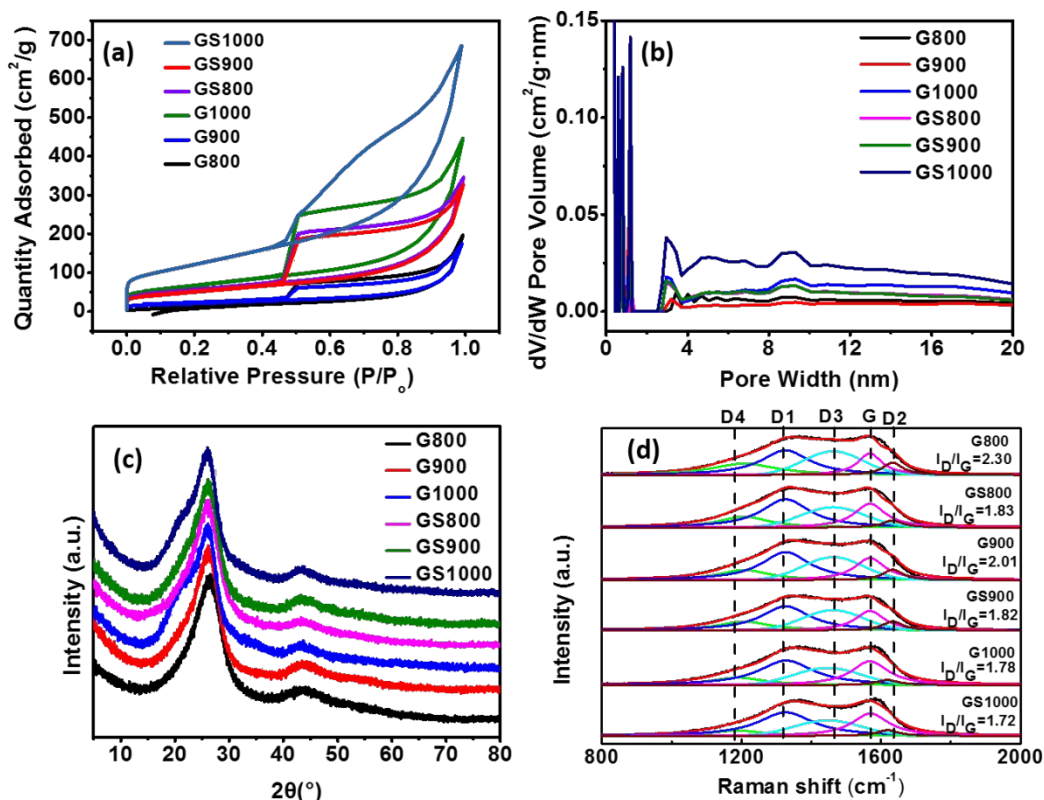


**Figure 3.** (a) N<sub>2</sub> adsorption/desorption isotherms; (b) Pore size distribution curves; (c) Powder X-ray diffraction patterns; (d) Raman spectra.

The nitrogen sorption behavior was measured to probe the porous structure of the as-synthesized samples (Figure 3). Besides the common microporous regions, all the samples present remarkable hysteresis loops at  $P/P_0 > 0.45$ , indicating the developed mesoporous properties. When the samples synthesized at the same temperature, GSX possesses more developed porosity than that of GX, suggesting the pore-forming effect of pre-ionization process by H<sub>2</sub>SO<sub>4</sub>. Moreover, higher temperature results in more desirable porous structure. G1000 and GS1000 have larger specific surface area up to

237 m<sup>2</sup> g<sup>-1</sup> and 427 m<sup>2</sup> g<sup>-1</sup>, respectively. The total pore volumes of G1000 and GS1000 are 0.49 cm<sup>3</sup> g<sup>-1</sup> and 0.75 cm<sup>3</sup> g<sup>-1</sup>, wherein the proportions of mesopore volumes occupy up to 86% and 84%, respectively, which are very considerable. Thus, G1000 and GS1000 are expected to exhibit more ideal effect for the mass transfer.

As shown in Figure 3c, XRD patterns of all the samples have two peaks centered at ca. 26 ° and 43 °, which can be assigned to (002) and (100) crystal plane of graphite carbon, respectively. The wide peak shapes indicate the existence of abundant defective structure.<sup>50</sup> The structural defects of samples were further analyzed by Raman spectra (Figure 3d) and expressed by the ratio of D1 band to G band. The higher  $I_{D1}/I_G$  indicates that more defective structure exists in the carbon materials. The  $I_{D1}/I_G$  values of GSX are generally lower than those of GX synthesized under otherwise the identical condition, suggesting the dopant S has extra influence on the crystallinity of the generated carbon. Therefore, the XRD and Raman results combined with the SEM and TEM characterization indicate the ultrathin and defective nature of the as-prepared 2D carbon nanosheets.

**Table 1.** Textural properties and elemental compositions.

Sample	Porosity data				Elemental composition <sup>c</sup>				
	$S_{BET}$ [m <sup>2</sup> g <sup>-1</sup> ]	$V_{total}^a$ [cm <sup>3</sup> g <sup>-1</sup> ]	$V_{meso}$ [cm <sup>3</sup> g <sup>-1</sup> ]	$V_{micro}^b$ [cm <sup>3</sup> g <sup>-1</sup> ]	C	N	O	S	N1+N3( %)
G800	51.99	0.30	0.21	0	76.67	21.04	2.29	0	77.72
G900	60.71	0.19	0.14	0.01	87.21	10.39	2.4	0	79.73
G1000	237.52	0.49	0.42	0.03	93.46	4.75	1.79	0	69.91
GS800	180.08	0.36	0.30	0.02	79.88	15.54	4.12	0.46	74.53
GS900	193.43	0.37	0.31	0.02	86.57	9.72	3.31	0.41	78.39
GS1000	427.07	0.75	0.63	0.05	89.8	3.93	5.74	0.53	65.83

<sup>a</sup> From total N<sub>2</sub> uptake at  $P/P_0=0.95$ . <sup>b</sup> From the DFT method. <sup>c</sup> Determined by XPS, at%

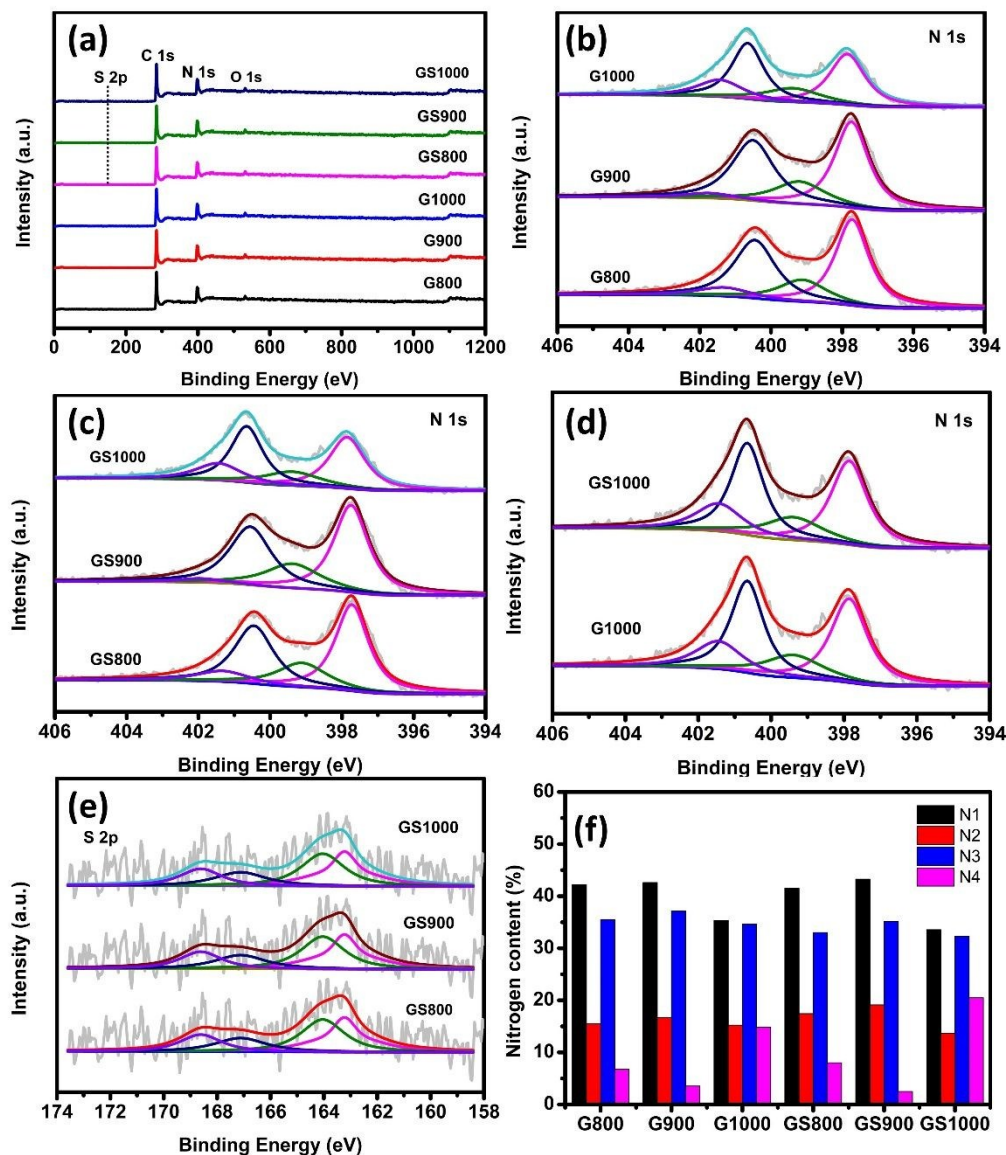


**Figure 4.** X-ray photoelectron spectroscopy. (a) Survey spectra; (b), (c), (d) N1s XPS spectra; (e) S 2p XPS spectra; (f) The content percentages of different nitrogen species.

The surface chemistry of the catalyst is an important parameter for the catalytic reaction, because it has great influence on the adsorption, desorption and activation of the substrate during the reaction. In order to understand the surface chemical properties of the catalyst, we used X-ray photoelectron spectroscopy (XPS) to detect the surface composition of the catalysts. As shown in Figure 4a, wide range scanning spectra indicate that C, N and O elements exist in all the catalysts, meanwhile S element is also

doped into GSX which is confirmed by the corresponding high resolution S 2p spectra (Figure 4e). The elemental composition determined by XPS is shown in Table 1. The high-resolution N1s spectra can be deconvoluted into four typical peaks located at 397.8, 399.3, 400.5, and 401.5 eV, respectively, belonging to N-1 (pyridine nitrogen), N-2 (pyrrole nitrogen), N-3 (graphitic nitrogen), and N-4 (nitrogen oxide)<sup>51</sup>. The ratios of four N species in different samples are shown in Figure 4f. According to previous studies, N-3 species play an important role at the activation of C-H.<sup>28</sup> We found that the total content of N species decreases with the increase of synthesis temperature, while the ratio of N-3 keeps relatively stable. The G1000 has a high N-3 ratio up to 34.59% in GX, and GS1000 has the same value 32.28% of N-3 ratio among GSX. Figure 4e shows the deconvolution results of high-resolution S 2p spectra of GSX, wherein the peaks at 163.2, 164.0, 167.1 and 168.6 eV belong to C-S-C (S 2p3/2), C-S-C (S 2p1/2), -C-SO<sub>x</sub>- (S 2p3/2) and -C-SO<sub>x</sub>- (S 2p1/2) bond, respectively.<sup>29, 36, 53</sup> The -C-S-C structure dominates in GS1000, while -C-SO<sub>x</sub>- dominates in both GS900 and GS800. -C-SO<sub>x</sub>- groups can serve as potential adsorption sites for the construction of S-O...H, leading to enhanced interaction with EB. Thus the distinct surface statuses are believed to exert different influences in catalytic reactions.

### Catalytic performance

To explore the catalytic potential of the presented carbons, we performed the liquid phase EB selective oxidation reaction catalyzed by these carbons under the same reaction condition. As shown in Table 2, TBHP can hardly oxidize EB in the absence of catalyst (Table 2, Entry 1). When oxidized carbon tubes (OCNT) and commercial graphene were used as catalysts, the EB conversion was below 15%, together with quite low selectivity for AcPO (45%), which indicating low performance of these two nanocarbons. In comparison, when different graphene-like GX and GSX samples were introduced, they exhibit notable enhanced catalytic performance. Moreover, the performance can be

further improved with the elevation of synthesis temperature independent of S doping. Figure 5a compares the reactivity of as-synthesized carbons with OCNT and commercial graphene. We can see that the prepared carbon nanosheets show a high catalytic performance with 85% EB conversion and 98% selectivity of AcPO, which is 8.5 times in conversion and 3.2 times in selectivity higher than OCNT under identical condition. Moreover, the catalytic performance of S-doped carbon nanosheet is obviously better than that of GX (without S doped) synthesized under the same condition. The EB conversion and AcPO selectivity reach up to 99% over GS1000 catalyst after 6 h reaction, indicative of effectively C-H activation ability of our predesigned carbon nanosheets. The participation of S changes the electrical characteristics and surface functional groups of the catalyst surface, which is responsible for improved chemical properties. Since GS1000 seems to be the best catalyst among all of the samples, we used it as a reference and optimized the reaction conditions. As can be seen from Table 2, high conversion as well as high AcPO selectivity can be obtained in the GS1000 catalyst by changing of reaction time and temperature, which are much better than other carbon-based benchmark catalysts.

The catalytic stability of catalysts is a very important indicator in industrial applications. To this purpose, we explored the recyclability of GS1000 for EB oxidation under the optimal reaction conditions. As shown in Figure 5b, after five times of reaction, there is minimal deactivation in the activity and selectivity, indicative of good stability of the catalyst GS1000 under current mild reaction condition.

On the basis of the preliminary success of the EB oxidation with TBHP as the oxidant, we also studied the oxidation of substituted aromatic hydrocarbons. Since GS1000 was found to be the best catalyst for EB oxidation, it was used in subsequent experiments, and the experimental results are shown in Table 3. GS1000 can effectively catalyze the oxidation of various benzyl aromatic hydrocarbons into corresponding ketone products, with the conversion ranging from 72% to 99%, and selectivity almost

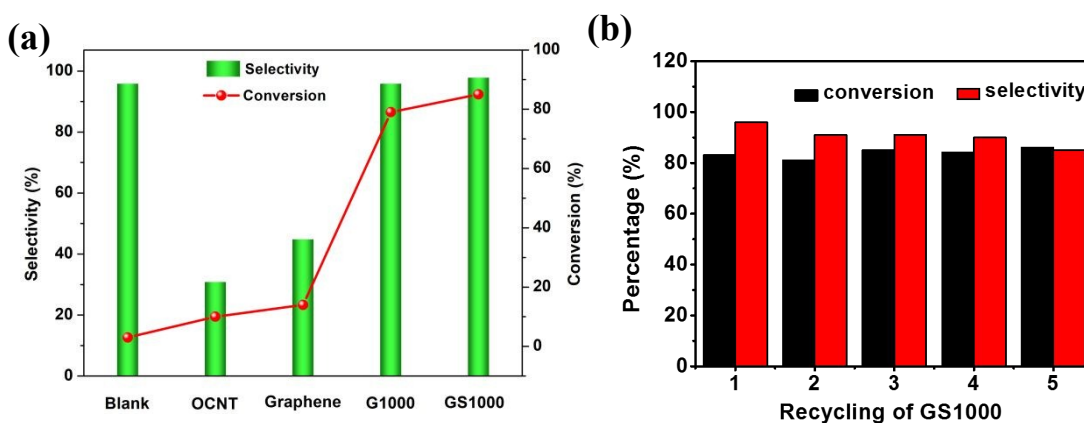
over 95%. Both electron-donor MeO- and electron-acceptor -NO<sub>2</sub> substituted substrates have relatively good conversion and selectivity. Aromatic substrates with large volume or steric hindrance also have good conversion, such as propyl benzene, isopropyl benzene, butyl benzene, iso-butyl benzene, diphenylmethane, fluorene and so on. This indicates that our new metal-free catalyst is applicable to the phenyl substrate.

**Table 2.** Screening of catalysts and optimization of reaction conditions

Entry	Catalyst	Temp. (°C)	T (h)	Conv. (%)	Sel. (%)
1	Blank	80	4h	3	96
2	OCNT	80	4h	10	31
3	Graphene	80	4h	14	45
4	G800	80	4h	8	70
5	G900	80	4h	28	83
6	G1000	80	4h	79	96
7	GS800	80	4h	24	82
8	GS900	80	4h	83	95
9	GS1000	80	4h	85	98
10	GS1000	80	2h	68	95
11	GS1000	80	5h	92	99
12	GS1000	80	6h	>99	>99
13	GS1000	60	4h	69	79
14	GS1000	100	4h	99	97
15	5 mg (98%) H <sub>2</sub> SO <sub>4</sub>	80	4h	0	-
16	Guanine	80	4h	0	-

Reaction condition: 10 mg catalyst, 1 mmol ethylbenzene, 2 mL H<sub>2</sub>O, 1 mL TBHP.

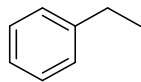
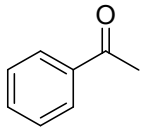
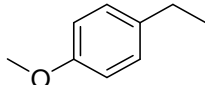
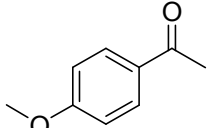
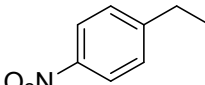
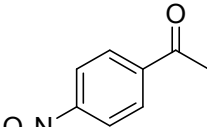
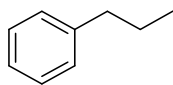
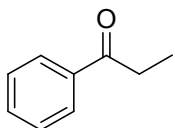
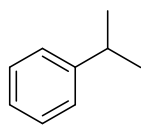
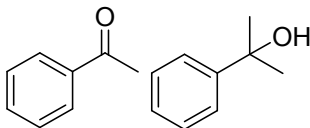
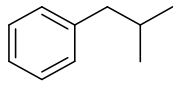
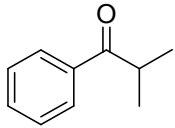
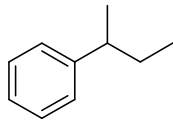
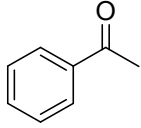
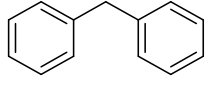
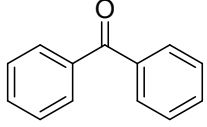
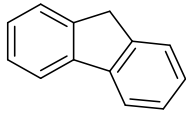
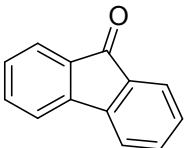
As revealed above, the activities of GSX all got improved compared to that of GX at different degrees. Based on available data, it can be reasonable to propose that both S-doping and the developed porosity are responsible for the remarkably enhanced activity. Among various N dopants, graphitic N have been demonstrated to be the most efficient dopant for improving the activity of carbon-based materials, which has been confirmed by the previous report<sup>4, 28</sup>. In our case, with the increase of the synthesis temperature, the ratio of N3 appears relatively constant (Figure 4f), but the activity of the catalyst increased significantly (Table 2), indicating that graphitization degree and surface areas could play more pronounced role for EB oxidation. In contrast to G1000, the GS1000 has similar N configuration, while it shows superior activity (see Table 1 and 2). The enhanced activity could be induced by N/S codoped effect from the incorporation of S dopant. XPS results indicate the presence of -C-SO<sub>x</sub> groups, which could facilitate the adsorption of EB by -S-O...H interaction, which is confirmed by calculation below.

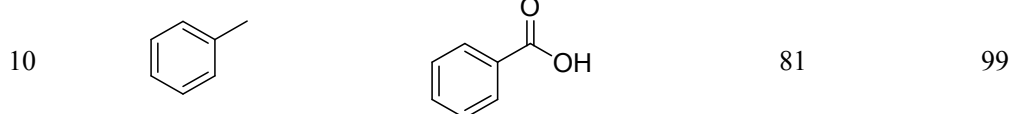


**Figure 5.** (a) activity comparison of respective catalysts, (b) the recycling test of GS1000 for ethylbenzene oxidation.



**Table 3.** The conversion of substituted aromatic hydrocarbons to corresponding ketone with GS1000 as catalyst.

Entry	Substrates	Products	Conversion(%)	Selectivity(%)
1			85	98
2			83	99
3			87	97
4			99	97
5			99	32 (ketone) 68 (alcohol)
6			72	99
7			81	99
8			82	99
9			81	99



Reaction condition: 1 mmol substrate, 10 mg catalyst, 1 mL TBHP (70%), 2 mL H<sub>2</sub>O, 80 °C, 4h

### Reaction mechanism

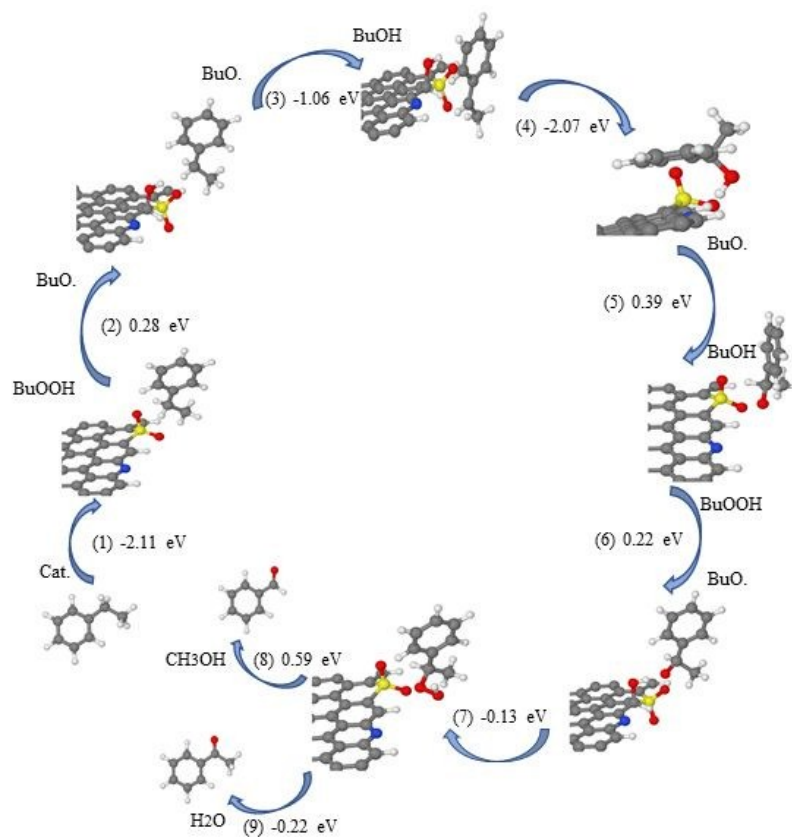


**Figure 6.** The elementary steps of OH radical mechanism for the ethylbenzene oxidation on pyridinic N and S codoped carbon nanosheet catalyst (p-N/S).

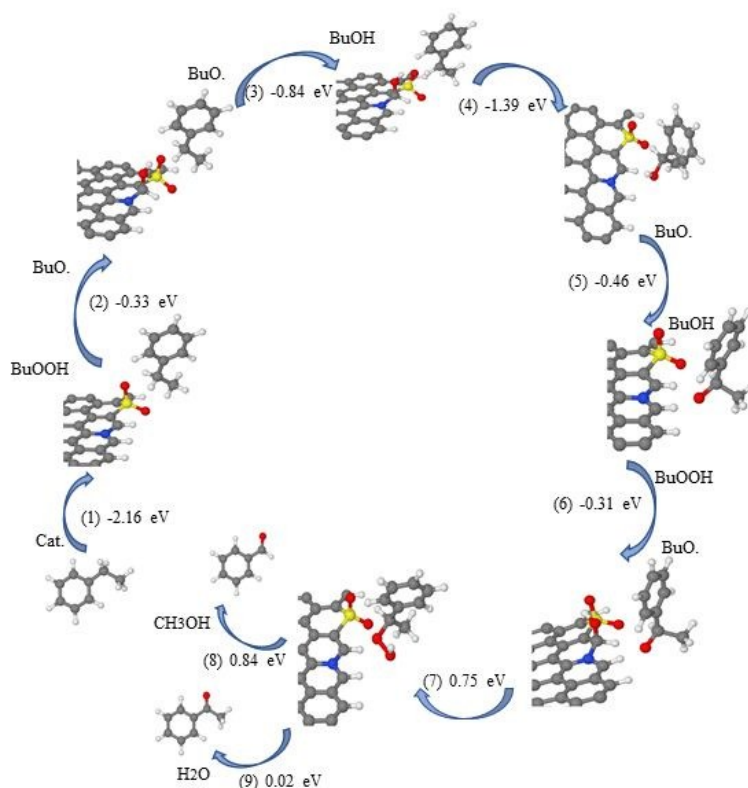


**Figure 7.** The elementary steps of OH radical mechanism for the ethylbenzene oxidation on graphitic N and S codoped carbon nanosheet catalyst (g-N/S).

To understand the origin of catalytic activity, the free radical scavenger p-benzoquinone was added to the catalytic system. Negligible conversion of EB was observed after the addition of p-benzoquinone, indicating the aliphatic C-H oxidation process in EB over GS1000 follows a free radical mechanism, which is in agreement with previous reports.<sup>52</sup> DFT simulations were performed for S/N co-doped graphene nanosheet catalysts. The S doped at graphene edges is oxidized and the N can be doped as pyridinic N (p-N) or graphitic N (g-N), which are named as p-N/S and g-N/S catalysts, respectively. There are also two possible mechanisms for the oxidation of ethylbenzene, namely, OH radical and OOH radical mechanisms, respectively. The OH radical mechanism for p-N/S and g-N/S catalysts are shown in Figure 6 and 7, and the OOH radical mechanism for p-N/S and g-N/S catalysts are shown in Figure S1 and S2 in

Supporting Information. As shown in Figure 6, we can find that ethylbenzene molecule is adsorbed on the oxidized S group by Van der Waals interactions (step (1)), which is a favorable exothermic process. The OH radical is formed via BuOOH and BuO., and subsequently adsorbed on edge site close to p-N (step (2) and (6)). However, this step is slightly endothermic for p-N/S catalysts. The step for 1-phenylethyl alcohol to 1-ethylbenzene oxygen radical (step (5)) is also slightly endothermic. The rest steps are exothermic and favorable for oxidation of ethylbenzene on p-N/S catalysts. As shown in Figure 7, it also indicates that the oxidized S group is favorable for adsorption of ethylbenzene. It is notable that all the elementary steps for g-N/S catalyst are exothermic till the formation of 1-hydroperoxyethylbenzene intermediate (step (7)). However, this step is favorable for p-N/S catalyst as shown in Figure 6. So, the best reaction mechanism should be the synergic effect of p-N/S and g-N/S catalysts, that is, g-N/S catalyst is favorable for the steps (1)-(6) while the g-N/S catalyst is responsible for the rest steps. The results for OOH radical mechanism for p-N/S and g-N/S catalysts are shown in Figure S1 and S2 in Supporting Information. For both catalysts, we can find that the second step for formation and adsorption of OOH radical is highly endothermic. So, the OOH radical mechanism is impossible, and the oxidation of ethylbenzene is catalysed by synergic effect of p-N/S and g-N/S catalysts via OH radical mechanism.

## Conclusion

Through direct carbonization of the pre-selected bioprecursor or its sulfate, a kind of thin N and N/S codoped carbon nanosheets can be obtained. Due to the stability of the bioprecursor nucleobases, carbon bond formation is restricted to result in a high local order carbon which as such are highly sp<sup>2</sup>-conjugated, heteroatom-doped carbons. The successful doping of S leads to the formation of “noble” carbon with more defects and optimized electronic configuration. With TBHP as oxidant, these noble carbon performs high activity to selective oxidation of C-H. Benefiting from the textural structure of the

noble carbons, such as ultrathin thickness, optimal porosity, rich structural defects and synergistic coupling effect of multiple dopants, GS1000 delivers superior catalytic performance for selective oxidation of ethylbenzene with good stability, and the applicability for the oxidation of the substituted phenyl substrate. It was proved that GS1000 catalyzed ethylbenzene oxidation is a OH radical reaction. The improved activity is likely due to the fact that the resulting electron-deficient sites from N/S codoping enhance the adsorption ability towards TBHP and smooth electron transfer on the surface of carbons. DFT calculation indicates that the oxidation of ethylbenzene is catalysed by synergic effect of p-N/S and g-N/S catalysts. The present work may open a new avenue for rational design and massive synthesis of heteroatom-doped 2D carbons as efficient metal-free catalysts for applications in selective oxidation.

### Acknowledgements

This work is financially supported by the National Natural Science Foundation of China (21571035), the Min Jiang scholar professorship Project, and the Strategic Priority Research Program of the Chinese Academy of Sciences (Grant No. XDB20000000).

### References

1. J. Zhang, X. Liu, R. Blume, A. Zhang, R. Schlogl and D. S. Su, *Science*, 2008, **322**, 73-77.
2. M. Christmann, *Angew. Chem. Int. Ed.*, 2008, **47**, 2740-2742.
3. Q. H. Xie, H. M. Zhang, J. C. Kang, J. Cheng, Q. H. Zhang and Y. Wang, *ACS Catal.*, 2018, **8**, 4902-4916.
4. B. Liu and Z. H. Zhang, *ACS Catal.*, 2016, **6**, 326-338.
5. Z. Guo, B. Liu, Q. H. Zhang, W. P. Deng, Y. Wang and Y. H. Yang, *Chem. Soc. Rev.*, 2014, **43**, 3480-3524.
6. R. G. Bergman, *Nature*, 2007, **446**, 391.
7. A. G. Macedo, S. Fernandes, A. A. Valente, R. A. S. Ferreira, L. D. Carlos and J. Rocha, *Molecules*, 2010, **15**, 747-765.
8. Y. Hirai, T. Kojima, Y. Mizutani, Y. Shiota, K. Yoshizawa and S. Fukuzumi, *Angew. Chem. Int.*

*Ed.*, 2008, **47**, 5772-5776.

9. R. P. Doherty, J. Krafft, C. Methivier, S. Casale, H. Remita, C. Louis and C. Thomas, *J. Catal.*, 2012, **287**, 102-113.
10. L. Kesavan, R. Tiruvalam, M. H. A. Rahim, M. I. Saiman, D. I. Enache, R. L. Jenkins, N. Dimitratos, J. A. Lopez Sanchez, S. H. Taylor and D. W. Knight, *Science*, 2011, **331**, 195-199.
11. P. Zhang, Y. Gong, H. Li, Z. Chen and Y. Wang, *Nat. Commun.*, 2013, **4**, 1593.
12. X. Lin, Z. Nie, L. Zhang, S. Mei, Y. Chen, B. Zhang, R. Zhu and Z. Liu, *Green Chem.*, 2017, **19**, 2164-2173.
13. X. Lin, S. Zhao, Y. Chen, L. Fu, R. Zhu and Z. Liu, *J. Mol. Catal. A-Chem.*, 2016, **420**, 11-17.
14. A. K. Suresh, M. M. Sharma and T. Sridhar, *Ind. Eng. Chem. Res.*, 2000, **39**, 3958-3997.
15. V. Georgakilas, J. A. Perman, J. Tucek and R. Zboril, *Chem. Rev.*, 2015, **115**, 4744-4822.
16. D. S. Su, G. Wen, S. Wu, F. Peng and R. Schlogl, *Angew. Chem. Int. Ed.*, 2017, **56**, 936-964.
17. K. Zhou, B. Li, Q. Zhang, J. Huang, G. Tian, J. Jia, M. Q. Zhao, G. Luo, D. S. Su and F. Wei, *ChemSusChem*, 2014, **7**, 723-728.
18. M. Antonietti, N. Lopez-Salas and A. Primo, *Adv. Mater.*, 2019, **31**.
19. G. Wen, Q. Gu, Y. Liu, R. Schlogl, C. Wang, Z. Tian and D. S. Su, *Angew. Chem. Int. Ed.*, 2018, **57**, 16898-16902.
20. Y. Ding, X. Huang, X. Yi, Y. Qiao, X. Sun, A. Zheng and D. Su, *Angew. Chem. Int. Ed.*, 2018, **57**, 13800-13804.
21. F. Chen, W. Li, B. Sahoo, C. Kreyenschulte, G. Agostini, H. Lund, K. Junge and M. Beller, *Angew. Chem. Int. Ed.*, 2018, **57**, 14488-14492.
22. J. Zhu, T. Diao, W. Wang, X. Xu, X. Sun, S. A. C. Carabineiro and Z. Zhao, *Appl. Catal. B-Environ.*, 2017, **219**, 92-100.
23. C. Tang and Q. Zhang, *Adv. Mater.*, 2017, **29**, 1604103.
24. J. X. Zhang, L. Qu, G. Shi, J. Liu, J. Chen and L. Dai, *Angew. Chem. Int. Ed.*, 2016, **55**, 2230-2234.
25. B. Frank, J. Zhang, R. Blume, R. Schlogl and D. S. Su, *Angew. Chem. Int. Ed.*, 2009, **48**, 6913-6917.
26. D. Begin, G. Ulrich, J. Amadou, D. S. Su, C. Phamhuu and R. Ziesel, *J. Mol. Catal. A-Chem.*, 2009, **302**, 119-123.
27. D. S. Su, S. Perathoner and G. Centi, *Chem. Rev.*, 2013, **113**, 5782-5816.
28. Y. Gao, G. Hu, J. Zhong, Z. Shi, Y. Zhu, D. S. Su, J. Wang, X. Bao and D. Ma, *Angew. Chem. Int. Ed.*, 2013, **52**, 2109-2113.

29. S. Yang, L. Peng, P. Huang, X. Wang, Y. Sun, C. Cao and W. Song, *Angew. Chem. Int. Ed.*, 2016, **55**, 4016-4020.
30. B. Huang, Y. Liu, X. Huang and Z. Xie, *J. Mater. Chem. A*, 2018, **6**, 22277-22286.
31. M. Titirici, R. J. White, N. Brun, V. L. Budarin, D. S. Su, F. D. Monte, J. H. Clark and M. J. MacLachlan, *Chem. Soc. Rev.*, 2015, **44**, 250-290.
32. R. Arrigo, M. E. Schuster, Z. Xie, Y. Yi, G. Wowsnick, L. Sun, K. Hermann, M. Friedrich, P. Kast and M. Havecker, *ACS Catal.*, 2015, **5**, 2740-2753.
33. Y. Gao, P. Tang, H. Zhou, W. Zhang, H. Yang, N. Yan, G. Hu, D. Mei, J. Wang and D. Ma, *Angew. Chem. Int. Ed.*, 2016, **55**, 3124-3128.
34. W. Liu, C. Wang, F. Herold, B. J. M. Etzold, D. S. Su and W. Qi, *Appl. Catal. B-Environ.*, 2019, **258**.
35. Z. Y. Li, Q. M. Gao, X. Liang, H. Zhang, H. Xiao, P. Xu and Z. P. Liu, *Carbon*, 2019, **150**, 93-100.
36. X. Hu, Y. Chen, B. Huang, Y. Liu, H. Huang and Z. Xie, *ACS Sustain. Chem. Eng.*, 2019, **7**, 11369-11376.
37. C. Tang, H. Wang, X. Chen, B. Li, T. Hou, B. Zhang, Q. Zhang, M. Titirici and F. Wei, *Adv. Mater.*, 2016, **28**, 6845-6851.
38. S. Li, C. Cheng, H. W. Liang, X. L. Feng and A. Thomas, *Adv. Mater.*, 2017, **29**.
39. W. Qi, P. Q. Yan and D. S. Su, *Acc. Chem. Res.*, 2018, **51**, 640-648.
40. X. L. Guo, W. Qi, W. Liu, P. Q. Yan, F. Li, C. H. Liang and D. S. Su, *ACS Catal.*, 2017, **7**, 1424-1427.
41. W. Qi, W. Liu, X. L. Guo, R. Schlogl and D. S. Su, *Angew. Chem. Int. Ed.*, 2015, **54**, 13682-13685.
42. W. Qi and D. S. Su, *ACS Catal.*, 2014, **4**, 3212-3218.
43. B. B. Huang, M. Xia, J. G. Qiu and Z. L. Xie, *ChemNanoMat*, 2019, **5**, 682-689.
44. Y. Oaki, S. Kaneko and H. Imai, *J. Mater. Chem.*, 2012, **22**, 22686-22691.
45. B. B. Huang, X. Hu, Y. C. Liu, W. Qi and Z. L. Xie, *J. Power Sources*, 2019, **413**, 408-417.
46. Y. C. Liu, B. B. Huang, X. F. Zhang, X. Huang and Z. L. Xie, *J. Power Sources*, 2019, **412**, 125-133.
47. P. Giannozzi, S. Baroni, N. Bonini, M. Calandra, R. Car, C. Cavazzoni, D. Ceresoli, G. L. Chiarotti, M. Cococcioni, I. Dabo, A. Dal Corso, S. de Gironcoli, S. Fabris, G. Fratesi, R. Gebauer, U. Gerstmann, C. Gougoussis, A. Kokalj, M. Lazzeri, L. Martin-Samos, N. Marzari, F. Mauri, R. Mazzarello, S. Paolini, A. Pasquarello, L. Paulatto, C. Sbraccia, S. Scandolo, G. Sclauzero, A. P.

- Seitsonen, A. Smogunov, P. Umari and R. M. Wentzcovitch, *J. Phys. Condens. Mat.*, 2009, **21**.
48. J. P. Perdew, K. Burke and M. Ernzerhof, *Phys. Rev. Lett.*, 1996, **77**, 3865-3868.
49. V. Barone, M. Casarin, D. Fopper, M. Pavone, M. Sami and A. Vittadini, *J. Comput. Chem.*, 2009, **30**, 934-939.
50. L. Yu, C. Falco, J. Weber, R. J. White, J. Y. Howe and M. Titirici, *Langmuir*, 2012, **28**, 12373-12383.
51. L. Lai, J. R. Potts, D. Zhan, L. Wang, C. K. Poh, C. Tang, H. Gong, Z. Shen, J. Lin and R. S. Ruoff, *Energy and Environ. Science*, 2012, **5**, 7936-7942.
52. K. Qu, Y. Zheng, S. Dai and S. Qiao, *Nano Energy*, 2016, **19**, 373-381.
53. W. Liu, L. Zhang, X. Liu, X. Liu, X. Yang, S. Miao, W. Wang, A. Wang and T. Zhang, *J. Amer. Chem. Soc.*, 2017, **139**, 10790-10798.

## Table of contents

